HIGH-ENERGY ION LINACS BASED ON SUPERCONDUCTING SPOKE CAVITIES

K. W. Shepard and P. N. Ostroumov

Physics Division, Argonne National Laboratory, 9700 S. Cass Avenue, Argonne, IL 60439

J. R. Delayen

Thomas Jefferson National Accelerator Facility, 12000 Jefferson Avenue, Newport News, VA 23606

The applicability of superconducting TEM-class spoke cavities to high-energy ion linacs is discussed, and detailed designs for two TEM-class, triple-spoke-loaded superconducting niobium resonant cavities are presented. The 345 MHz cavities have a velocity range of $0.4 < \beta < 0.75$ and a beam aperture of 4 cm. Spoke-loaded cavities offer several advantages compared with the higher-frequency elliptical-cell cavities that are currently being developed for this range of particle velocities. The proposed triple-spoke cavities can provide broader velocity acceptance, more accelerating voltage per cavity, reduced heat load, operation at 4.5 K, and increased longitudinal acceptance through the high-energy section. Application to the proposed RIA driver linac is discussed in detail.

1 Introduction

We compare TEM-class, superconducting spoke-loaded resonant cavities [1-3] for a high-energy superconducting (SC) ion linac with TM, elliptical-cell cavities, as are being employed, for example, in the proton driver linac for the SNS project [4]. An illustrative application examined in detail is the high-energy section of the driver linac for the proposed U.S. rare-isotope facility (RIA) [5.6]. The RIA driver is required to produce uranium beams at 400 MeV per nucleon and, additionally, beams of lighter ions at as high an energy as possible.

2 Properties of Cavity Geometries

Two main classes of SC cavity are under consideration for the medium-β region. The first class is based on a groups of several cylindrical cells operating in the cylindrically symmetrical TM_{010} mode. This class is topologically identical to the one used at $\beta=1$, but with a reduced cell length [7-9]. The other class is based on singly- or multiply-loaded structures where each loading element supports a TEM mode. Included in this class are the types of cavities that are used extensively in the low-β region [10,11]. We will refer to these

two classes of cavity geometry as TM and TEM geometries, respectively. TEM and TM cavity geometries differ in three major respects: the transverse dimensions, the cell-to-cell coupling and the localization of the electromagnetic field [12,13].

The transverse dimension of TM structures is of the order of 0.9 λ while for TEM structures it is of the order of 0.5 λ, where λ is the free-space wavelength of the accelerating mode. Thus, at the same frequency, TEM structures have about half the transverse size of TM structures. Alternatively, at the same transverse size, they will operate at about half the frequency. Since the BCS surface resistance of superconductors is quadratic with frequency, TEM structures operating at lower frequency will require less refrigeration and have the potential to operate at higher temperatures. Additionally, at half the frequency, a TEM structure will have half the number of cells of a TM cavity of the same length; and thereby will offer a broader velocity acceptance or better efficiency in accelerating particles over a range of velocities. Operating at lower frequency also has advantages from a beam physics perspective that will be explored further in following sections.

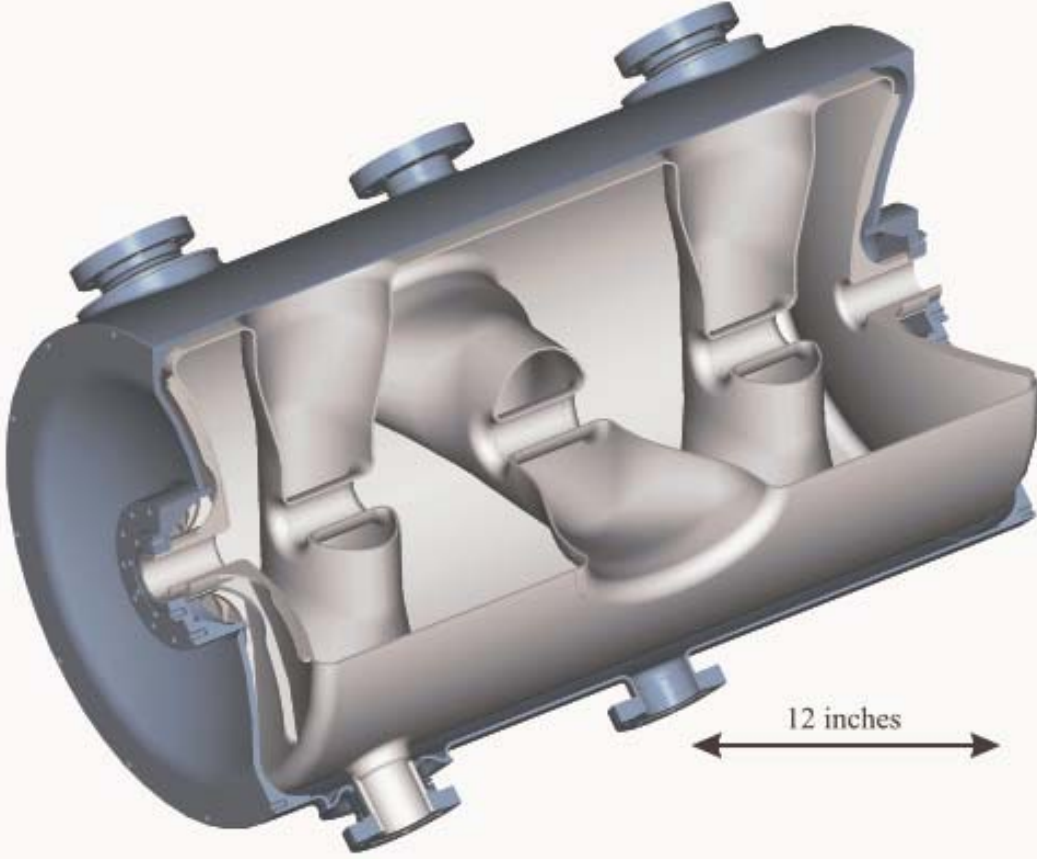In TM cavities the cell-to-cell coupling takes place through the beam-line irises. In

Figure 1: Sectioned view of a 345 MHz triple-spoke-loaded cavity for $\beta_{GEOM} = 0.50$. The niobium cavity shell is nested in a stainless-steel jacket, which provides containment for 4.5K liquid helium.

order to provide sufficient coupling, the iris opening needs to be sufficiently large. Increasing the iris diameter has two consequences: it increases the surface fields and, when the iris size becomes comparable to the cell length, it reduces the on-axis accelerating field for a given energy content and power dissipation, leading to a reduction of the shunt impedance of the cavity. For this reason, the cell-to-cell coupling in TM cavities is often less than 2%, making them sensitive to geometrical deformation and requiring accurate, tight-tolerance mechanical tuning to obtain a flat field profile. For TEM cavities, on the other hand, all the cells are strongly coupled by the rf magnetic field, with cell-to-cell coupling typically on the order of 20 to 30%. Such a large cell-to-cell coupling results in a fundamental mode with large frequency spacing from any other rf modes, and in a geometry that is robust with respect to mechanical tolerance. For this reason tuning of the multiple spoke cavities after fabrication in order to obtain a flat field profile is not necessary, since typical fabrication errors will not appreciably affect the field profile.

In TM structures the electromagnetic field varies slowly over position in the cavity, and the electromagnetic field-level is relatively high over a large volume, resulting in a large energy content for a given accelerating gradient. In TEM cavities, on the other hand, not only is the volume smaller at a given frequency, but high electromagnetic fields are confined to the regions along the beam line and along the loading elements. This results in a lower energy content at a given frequency and gradient, which has two consequences. The first is reduced power dissipation in the cavity walls or higher shunt impedance. The second is that less rf power is required to phase stabilize the rf fields under the influence of microphonics-induced frequency variations.

Table 1: Geometric parameters of the two types of triple-spoke cavities. The radius of the spherical end-walls is 40 cm, and all blend radii are 1.27 cm.

Geometric Beta		$\beta_{GEOM} = 0.50$		$\beta_{GEOM} = 0.62$	
Diameter of housing		21.7 cm		22.9 cm	
Interior length of housing		67 cm		85 cm	
Beam Aperture		4.0 cm		4.0 cm	
Elliptical Spoke Diameters		End spokes	Central Spoke	End spokes	Central Spoke
Central region	Longitudinal	5.0 cm	5.6 cm	6.25 cm	7.4 cm
	Transverse	8.0 cm	8.0 cm	8.75 cm	9.4 cm
At cavity wall	Longitudinal	7.5 cm	10.0 cm	10.0 cm	12.0 cm
	Transverse	6.5 cm	5.6 cm	7.0 cm	7.0 cm

The lower energy content of TEM cavities at a given frequency opens a possibility to design and operate a linac at lower frequency which, as discussed below, can provide numerous benefits..

There is a general perception that the peak surface electromagnetic fields at a given gradient are larger in TEM geometries than in TM geometries. Certainly this has been true historically when comparing low-velocity ($\beta<0.2$) TEM structures with high-velocity ($\beta=1$) TM structures. For TEM structures, however, the surface fields are relatively independent β, while for TM structures they increase significantly when β is reduced below 1. As a consequence, at intermediate velocities, say $\beta \approx$ 0.5-0.6, the surface fields for both types of geometries are pretty much the same [12].

We note that surface fields may not be a dominant factor in all cases: for example, for cw linacs, rf losses may prohibit cw operation at gradients higher than 10 MV/m [14].

3 Two Triple-Spoke Cavities

Designs for two SC niobium, 345 MHz, three-spoke-loaded cavities for the velocity range 0.4<β<0.75 have been developed. Figure 1 shows a sectioned view of one of the two cavity types. The mechanical elements and overall design are similar to those of a recently prototyped 345 MHz two-spoke niobium cavity [15]. The niobium elements of the cavity are formed of 3.18 mm thick niobium sheet, and housed in an integral stainless-steel jacket, which contains the liquid helium coolant.

In the three lowest-frequency rf eigenmodes, the three spoke elements behave as coupled, TEM-like half-wave-resonant lines. The lowest-frequency rf eigenmode is the accelerating mode, in which adjacent spokes are of opposing polarity.

The structures were modeled using Microwave Studio software [16]. A primary design objective was to minimize and balance the peak values of surface electric and magnetic fields in order to maximize the accelerating gradient as constrained by present state-of-the-art for niobium SC cavities. Table 1 details the geometric parameters for the two types of three-spoke resonant cavity (TSR) discussed below.

As can be seen in Figure 1, the spoke elements are elliptical in cross-section. In the central portion of the spoke, the major axis is perpendicular to the beam axis, in order to minimize the peak value of the surface electric field. As the spoke approaches the cylindrical outer wall, elliptical section is expanded and the major axis rotates 90 degrees, parallel to the beam axis, in order to minimize the peak surface magnetic field.

A crossed-spoke geometry has been chosen in which the central spoke is oriented at a right angle to the spokes at each end of the cavity .It is possible to achieve approximately the same peak surface fields with all three spokes parallel, but the parallel-spoke geometry results in the lowest-lying rf eigenmodes being very

closely spaced in frequency. The crossed-spoke geometry provides a large frequency spacing and maximizes the mechanical tolerances required to balance the electric fields in the three accelerating gaps. Also, the possibility of low-level multipacting coupling two rf modes is reduced with increased mode-splitting. For these reasons we have chosen the crossed-spoke geometry shown in Fig. 1.

Electromagnetic properties

Table 2 lists the principal electromagnetic parameters for the two 345 MHz triple-spoke-loaded cavities. Included for comparison are parameters for the two 805 MHz elliptical 6-cell cavities designed for the same particle velocities and which are part of the 'baseline' design for the RIA driver linac [6,17].

Figure 2 compares the velocity acceptance, i.e. the voltage gain per cavity as a function of particle velocity, of the triple-spoke and elliptical cell cavities. The accelerating field level is determined by setting the peak surface electric field at 27.5 MV/m for all the cavities, the feasibility of which is indicated by recent experimental results for a number of niobium spoke and elliptical cell cavities [15, 18-20]

Note that, because of the lower frequency enabled by using a TEM structure, the triple-spoke geometry provides significantly broader velocity acceptance and higher voltage gain than the elliptical cell option.
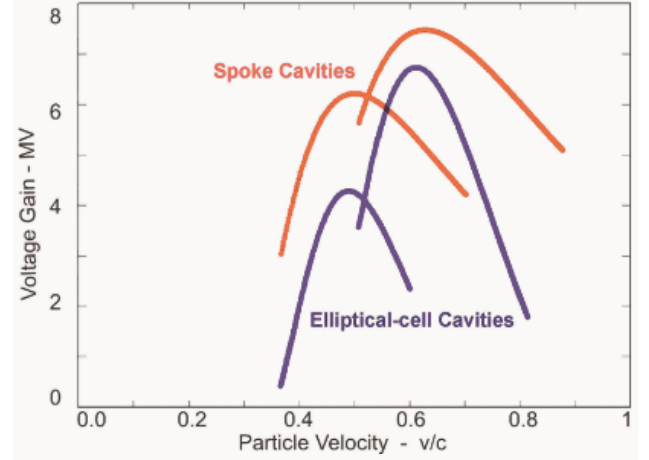

Figure 2: Velocity acceptance for two 345 MHz triple-spoke cavities compared with two 805 MHz elliptical 6-cell cavities, all operating at a peak surface electric field of 27.5 MV/m.

The breadth of velocity acceptance varies inversely with the number of cells (each of length $\beta\lambda/2$) incorporated into accelerating structure. The more cells, the more voltage gain per cavity, but the narrower the velocity acceptance. In the present case, for a given particle velocity, the cell length is a factor of 2.33 longer for the 345 MHz three-cell spoke cavities, which can therefore provide at the same time both more voltage and broader velocity acceptance than an 805 MHz six-elliptical-cell cavity. As is discussed below, using these two triple-spoke cavities we can span the required velocity range not only with

Cavity Type	Triple-Spoke	Elliptical Six-Cell	Triple-Spoke	Elliptical Six-Cell
Beta Geometric	0.50	0.47	0.62	0.61
Frequency (MHz)	345	805	345	805
Length (cm)	65.2	52.55	80.87	68.2
G	85.7	136.7	93.0	179.0
R/Q	494	160	520	279
at an accelerating gradient of 1 MV/m:				
RF Energy (mJ)	397	341	580	330
peak E-field (MV/m)	2.88	3.41	2.97	2.71
peak B-field (G)	86.5	69	88.6	57.2

Table 2: Electromagnetic parameters for the two triple-spoke cavities compared with two elliptical-cell 6-cell cavities of similar geometric β = v/c developed for the SNS linac and for the RIA driver linac.
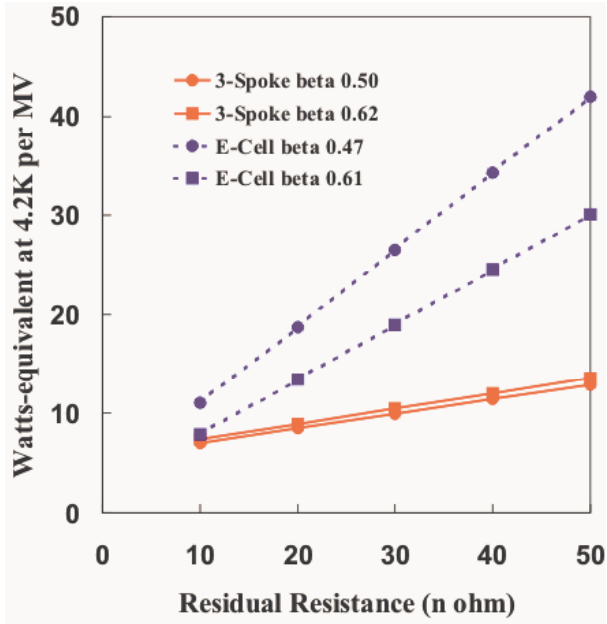
Figure 3: RF load into helium refrigeration as a function of cavity performance.

fewer cavities, but also with fewer types of cavity.

Cavity RF heat load

The excellent shunt impedance of the spoke-loaded cavities, together with the relatively low operating frequency, enables us to design the linac not only to reduce the RF heat load but also to operate at 4.3K.

Operation at 4.3K is impractical for the elliptical-cell cavities which, because of the very much higher surface resistance at 805 MHz, must operate at 2K. The lower-frequency TEM spoke cavities can be operated at 4.3 K, which eliminates the need for sub-atmospheric operation, substantially simplifying the cryogenic system. The refrigerator, distribution system, and linac cryostats would all be appreciably simpler to build, maintain, and operate at a temperature of 4.3K as opposed to 2K.

Figure 3 shows the RF heat load in watts per MV of accelerating potential for the 345 MHz triple-spoke cavities operating at 4.3K (solid lines). For comparison, we show the refrigeration load for the 805 MHz elliptical six-cell cavities operating at 2K (dashed lines). The 2K system is assumed to achieve an efficiency such that a 0.25 watts into 2K is equivalent to 1 watts of heat load into 4.3K

[21,22]. The heat load in Figure 3 is estimated assuming operation of all cavities at a peak surface electric field of 27.5 MV/m, as discussed above.

In Figure 3, the heat load is shown as a function of cavity performance specified in terms of an empirically determined residual resistance characterizing the quality of the SC cavities. The residual resistance R_{EXC} is taken to be the resistance required to be added to the BCS SC surface resistance R_{BCS} to account for the measured total rf loss (R_{EXC}+ R_{BCS}) at a given temperature and field level. Design goals recently quoted for elliptical-cell cavities range over $25<R_{EXC}<50$ nΩ for long-term, on-line performance [18,20]. At this performance level, the use of spoke-loaded cavities would reduce the refrigeration load per MV of linac by a factor of two or more relative to the higher-frequency elliptical-cell alternative.

Note that for the spoke cavities, the reduced slope of heat load as a function of residual resistivity provides a large design margin in terms of overall linac heat-load as contingent on a range of SC cavity performance.

4 Low-frequency Cavities and Reduced Beam Loss

Medium-energy high-power ion linacs, both those presently operating and those that are being constructed, use room-temperature drift-tube accelerating structures for velocities less than 0.6c [4, 23-26]. As is well known, the shunt impedance of drift-tube structures becomes low at velocities above 0.3c. At lower velocities, lower frequency structures are more efficient. In order to minimize the construction costs of a linac and to keep the operating efficiency high, the high-energy section (above 0.4c) is usually operated at a higher harmonic of the bunch frequency. The resultant frequency jump abruptly reduces the phase width of the stable area in longitudinal phase space, and as a consequence reduces the longitudinal acceptance.

The reduced acceptance can be a problem in high-power machines because of beam halo. Downstream of the frequency transition, some

halo particles are likely to be located outside of the longitudinally stable area. In the velocity range below ~0.55c-0.6c the focusing lattice usually provides stable motion only for the particles inside the separatrix. Halo particles outside of the separatrix can become unstable transversely and are then lost in the high-energy section of the linac. This mechanism can be a major source of beam loss in high-power linacs.

If, however, the frequency jump in ion linacs takes place above velocities ~0.6c, a wide range of particle momentum will be stable transversely and can be transported to the end of the linac even if particles are located outside of the longitudinally stable area. At sufficiently high velocities, transverse focusing is stable for a wide range of particle momentum due to the significant suppression of the defocusing term of the accelerating field. In this case, the lower energy particles can be transported all the way through the linac and successfully dumped in high dispersion area of the switchyard.

Different high-power machines have different mechanisms of halo formation. For example, in proton/H-minus linacs the main source of halo formation is the beam space-charge. In the case of the RIA driver linac discussed below, the main source of beam halo is scattering in the final, relatively thick stripping foil.

5 Spoke-Cavity High-energy Section for the RIA Driver Linac

The proposed U.S. rare isotope accelerator facility (RIA) requires a driver linac producing cw, 100 kW ion beams at energies of 400 keV/nucleon or more for all ion species. A baseline design for the driver linac has been developed which consists of an array of several types of independently-phased, short, SC accelerating structures [6,17]. In order to produce sufficiently intense beams the linac must accelerate multiple charge state beams of the heavier ions. This requirement largely drives the lattice design and beam dynamics for the linac.

We confine our discussion to the high-energy section of the linac which, for uranium beams, is between the final charge-stripping at 80 MeV/nucleon and the output at 400 MeV/nucleon. The high-energy section comprises approximately 2/3 of the overall linac, providing 780 MeV of acceleration. We compare two options: the baseline design, which employs three types of elliptical-cell 6-cell cavities, and a design using the two types of triple-spoke-loaded cavity described above, i.e. 350 MHz, β_G=0.5 and β_G=0.62c. In what follows we refer to the first option as the elliptical-cell linac (ECL) and the second option as the triple-spoke linac (TSL).

Cavity Type	Geometric Beta	Frequency MHz	Length cm	E_{PEAK} MV/m	E_{ACC} MV/m	Number of Cavities
Triple-spoke cavity option						
3 Spoke	0.50	345.0	65	27.5	9.5	42
3 Spoke	0.62	345.0	81	27.5	9.3	98
					Total # Cavities =	140
Elliptical-cell 6-cell cavity option						
6 Cell	0.47	805.0	55	27.5	8.1	60
6 Cell	0.61	805.0	68	27.5	9.9	88
6 Cell	0.81	805.0	91	27.5	12.6	32
					Total # Cavities =	180

Table 3: SC cavity arrays required for the high-energy section for the RIA driver linac for the two design options considered.

Table 4 Output beam energies (MeV/ nucleon) for several ion species for the two design options.

Species	Triple-spoke	Elliptical-cell
H	956	908
He^3	712	713
D	574	588
A^{40}	517	537
Xe^{136}	442	460
U^{238}	405	404

The cavity array is determined by the requirement to produce uranium beams at 400 MeV/nucleon. The uranium beam at the entrance to the high-energy section is at an energy of 81 MeV/nucleon and is composed of four charge states. Table 3 shows the number and types of cavities required, for each of the two design options, in order to accelerate the uranium beam to an energy of 400 MeV/nucleon. The TSL option requires substantially fewer cavities than the ECL design.

For lighter ions, the charge to mass ration is higher, and the cavity array can be tuned to output a higher energy beam, as shown in Table 4. One effect of the broader velocity acceptance of the triple-spoke cavities is to produce an appreciably higher-energy proton beam than the ECL design.

A focusing system with room-temperature quadrupole doublets located outside of the cryostat is used in the ECL 'benchmark' design and could be used for the TSL. We have chosen, however, to use 50 cm long, 9 Tesla SC solenoids in the TSL design. The solenoids provide strong transverse focusing for all ion beams and can be incorporated into the cryostats, economizing space along the beam-line.

A realistic accelerating-focusing lattice for the TSL high-energy section is based on two types of cryostat, as shown in Fig. 4. The first type is 3.4m in length and contains one SC solenoid and three β_G=0.5 triple-spoke cavities. The second type is 5.3m in length and contains one solenoid and four β_G=0.62 triple-spoke cavities. The space between the cryostats, approximately 0.5m, is adequate for beam diagnostics and beam steering magnets. We note that the latter could be integrated into the solenoids inside the cryostat. Table 5 summarizes and compares some of the principal parameters and features of the TSL and the ECL design options for the RIA driver linac high-energy section.

Beam Dynamics

Beam dynamics were studied and compared for both design options by numerical modeling using the code TRACK [27], which integrates the particle motions through 3D electromagnetic fields. The 3D RF electromagnetic fields
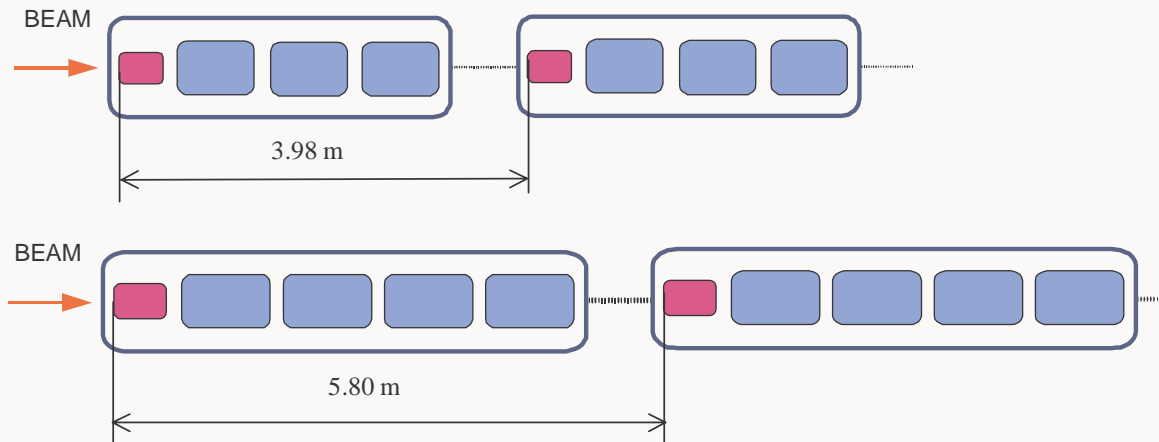

Figure 4. Layout of the cryostats containing two types of triple-spoke-loaded superconducting cavity: β_G=0.5 (top) and β_G=0.62 (bottom).

Table 5. Summary of the parameters for the two design options for the high-energy section of the RIA driver linac

Parameter	Triple-spoke	Elliptical-cell
Frequency (MHz)	345	805
Peak E field (MV/m)	27.5	27.5
No. of cavity types	2	3
Total no. of cavities	140	180
Temperature (K)	4.5	2.1
Aperture (mm)	40	80
Synchronous phase	-25	-30
Normalized Acceptance		
Trans. (π·mm·mrad)	35	70
Long. (π·keV/u-nsec)	280	60

were obtained using electrodynamics code CST Microwave Studio (Version 4.0). Both transverse and longitudinal rms beam sizes were carefully matched prior to detailed beam dynamics simulation..

The numerical simulation starts at the entrance of SC linac (beta=0.02) with a two-charge-state beam from the RFQ injector [28]. Multiple-charge state transport systems follow each of the two strippers. For uranium beam, the low-beta section accelerates 2 charge states,
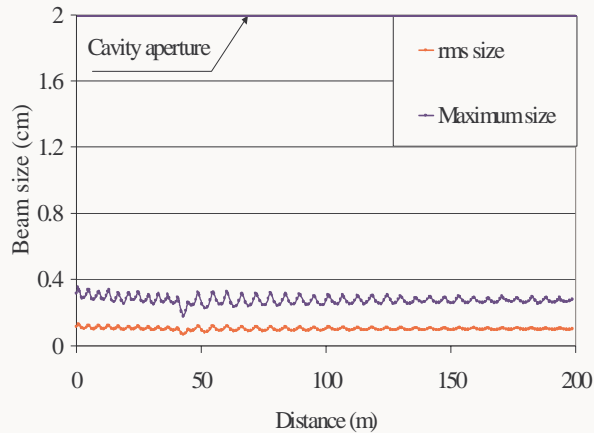
Figure 5. Rms beam size (the red curve) and maximum size (the blue curve) in the transverse horizontal plane through the high-β section of the triple-spoke cavity based linac.
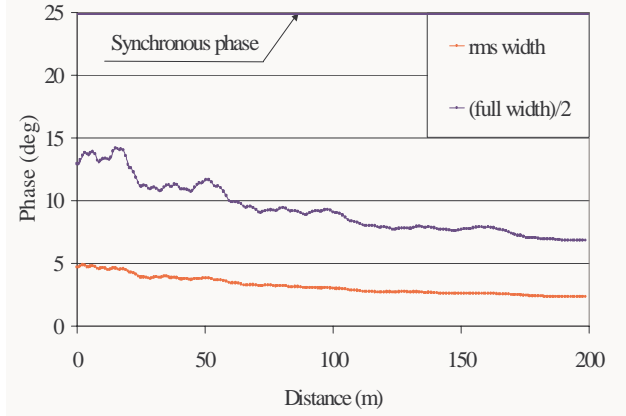
Figure 6. Rms beam size (the red curve) and maximum size (the blue curve) in the longitudinal plane through the high-β section of the triple-spoke cavity based linac.

28+ and 29+, to the first stripper and the medium beta section accelerates 5 charge states to the second stripper. After the second stripper, the four charge states 88-91+ are transported to the entrance of the high-energy section.

In the simulations, the synchronous phase for the ECL is set at –30°, while in the TSL it can be reduced to -25° because of the large longitudinal acceptance of the lower-frequency cavity array.

The simulation results shown are for 10^4 particles per bunch and include 30 seeds of random errors both in alignment of all elements (300 micron), and also in the phase and amplitude of the electromagnetic fields in the SC cavities. The latter errors were set at a maximum of ±1 degree and ±1% in the lowest frequency resonant cavities (58 MHz), and of ±0.5 degree and ±0.5% in all higher frequency resonators.

Figures 5 and 6 show the longitudinal and transverse beam envelopes through the high-energy section of the triple-spoke cavity based linac. The envelopes contain all four charge states. Both maximum size and rms size are plotted.

In Figure 7 the longitudinal acceptance for both the ECL and TCL designs, determined by Monte Carlo simulations, is outlined with blue dots. The red areas in Fig. 7 show, for both design options, the longitudinal phase-space of
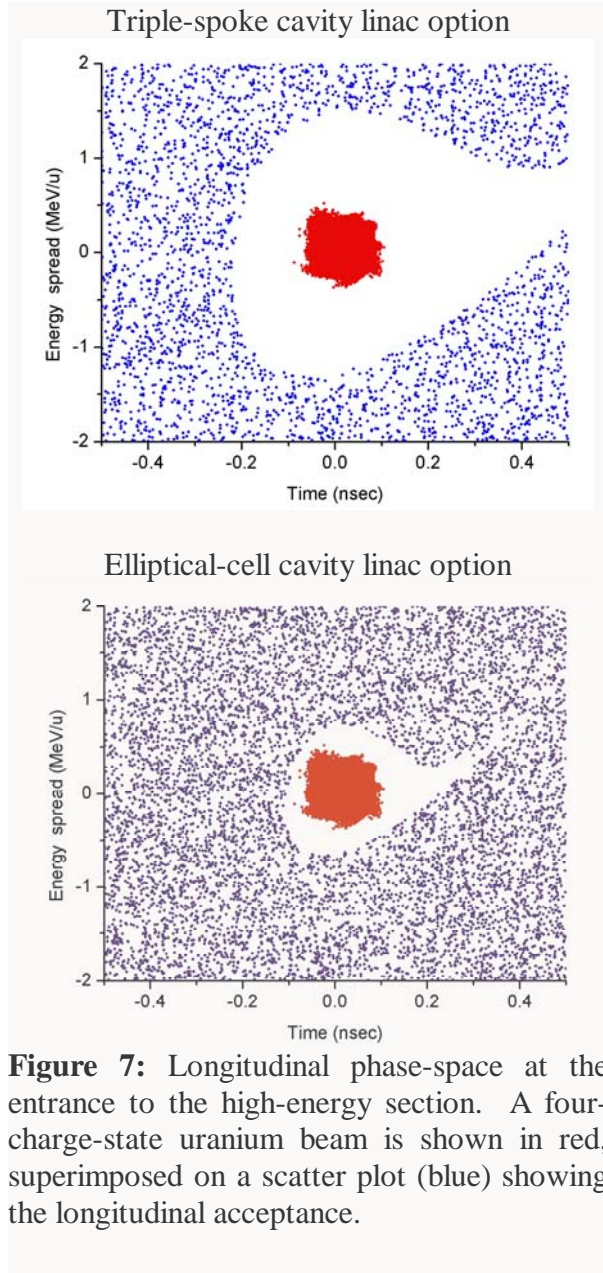
Figure 7: Longitudinal phase-space at the entrance to the high-energy section. A four-charge-state uranium beam is shown in red, superimposed on a scatter plot (blue) showing the longitudinal acceptance.

the four-charge-state uranium beam at the entrance of the high-energy section.

For the ECL design, the elliptical-cell iris diameter is set at 80 mm in order to provide adequate cell-cell coupling. Such a large aperture provides a very large transverse acceptance for this design option. The 40 mm beam aperture of the triple-spoke cavities provides, however, an ample safety factor in the transverse plane. Indeed, the aperture-to-rms-beam-size ratio, a critical factor for high-power linacs, remains in the range 16-20 throughout the TSL linac.

We note that the possibilities for beam loss are likely to be much more strongly impacted by the longitudinal rather than transverse acceptance, since the situation is more marginal in longitudinal phase space [29]. While the numerical studies reported to date indicate that both the baseline ECL and the TSL design options can provide good beam quality for multiple-charge-state beams, the reported studies have not included detailed simulation of the effects of scattering in the high energy stripping foil required for the heaviest ions.

Effects of stripping on beam halo

At the present time, experimental data characterizing the stripping process for high-power heavy-ion beams at energies ~85 MeV/u are not available. We note, however, that recent calculations for EURISOL [30], indicate the possibility of as much as several parts in 10^4 of the beam exhibiting extreme energy straggling on the low energy side. Because of the multiple charge state nature of the beam, it would be difficult to clean such a low energy tail in the chicane section following the stripper.

In the results shown in Figure 7, the stripping foil is simulated by SRIM [31], and the obtained standard deviations of transverse scattering and energy straggling are then used in the TRACK code for regeneration of the particle coordinates using Gaussian distribution in energy and scattered angles. The standard deviations are 17.6 keV/u (energy) and 0.5 mrad (angle). The stripping foil is assumed to fluctuate in thickness by a uniformly distributed ±2.5%. Such fluctuations can be caused by thermal deformations and by beam-induced sputtering of the foil itself. The thickness fluctuation contributes substantially to the emittance growth because the total energy loss is large: 3.29 MeV/u.

As was discussed in the previous section, a good method to avoid beam loss from the low energy tail is to provide large longitudinal acceptance in the high-energy section. The TSR design option achieves this to a much greater extent than the baseline ECR design,

which more than doubles the linac frequency right at the second stripper.

6 Conclusions

TEM-class, spoke-loaded superconducting cavities can provide an effective and efficient means of accelerating ion beams to velocities as high as 0.7c.

As applied to the RIA driver linac, spoke-loaded cavities provide a number of advantages compared with the higher-frequency, elliptical-cell cavities that have been proposed for this application. In particular, using TEM-class, spoke-loaded cavities:

1. Reduces the required number of cavities from 180 to 140.
2. Reduces the number of cavity types in the high-energy section from 3 to 2
3. Increases the operating temperature from 2 to 4.3 K
4. Reduces the refrigeration required by approximately a factor of two.
5. Increases the longitudinal acceptance by a factor of 4.7, decreasing the possibilities for beam loss and activation.

In addition, TEM-class spoke-loaded cavities have excellent mechanical stability, minimizing the difficulty of tuning and phase control.

7 Acknowledgements

8 References

1. J. R. Delayen, *Proc. 1988 Linear Accelerator Conference*, Williamsburg VA, October 3-7 1988, CEBAF-Report-89-001, p. 199.
2. J. R. Delayen, W. L. Kennedy, and C. T. Roche, *Proc. 1992 Linear Accelerator Conference*, edited by C. R Hoffmann, Ottawa CA, August 1992, AECL-10728, p. 695.
3. K. W. Shepard, M. Kedzie, J. R. Delayen, J. Mammosser, and C. Piller, *Proc. 1999 Particle Accelerator Conference*, New York NY, March 1999, IEEE Catalog No 99CH36366, p. 955.
4. M. White, "The Spallation Neutron Source (SNS)", *Proc. 2002 Linear Accelerator Conference,* Gyeongju, South Korea, August 2002.
5. J. A. Nolen, "The U.S. Rare Isotope Accelerator Project", *Proc. 2002 Linear Accelerator Conference,* Gyeongju, South Korea, August 2002.
6. K.W. Shepard, et al., *Proc. 9th Int. Workshop on RF Superconductivity*, Santa Fe, New Mexico, November 1999, p345.
7. G. Ciovati *et al, Proc. 2001 Particle Accelerator Conference,* Chicago, IL, June 2001, IEEE Catalog No. 01CH37268, p. 484.
8. T. Tajima *et al, Proc. 2001 Particle Accelerator Conference,* Chicago, IL, June 2001, IEEE Catalog No. 01CH37268, p. 1119.
9. C. C. Compton *et al, Proc. 2001 Particle Accelerator Conference,* Chicago, IL, June 2001, IEEE Catalog No. 01CH37268, p. 1044.
10. J. R. Delayen, in *Proc. 4th Workshop on RF Superconductivity,* Tsukuba, Japan, August 1989, KEK Report 89-21, p. 249.
11. K. W. Shepard, Nucl. Instr. and Meth. in Phys. Res. A 382 (1996), p. 125.
12. J. R. Delayen, "Medium-β Superconducting Accelerating Structures", *Proc. 10th Workshop on RF Superconductivity,* Tsukuba, Japan, September 2001.
13. S. H. Kim, "Challenges and the Future of Reduced-β SRF Cavity Design", *Proc. 2002 Linear Accelerator Conference,* Gyeongju, South Korea, August 2002.
14. W. J. Schneider, P. Kneisel, C. Rode, "Gradient Optimization for SC CW Accelerators", *Proc. 2003 Particle Accelerator Conference,* Portland, OR, May 2003.
15. J. Fuerst, M. Kedzie, M. Kelly, K. Shepard, "Superconducting 345 MHz Two-Spoke Cavity for RIA", *Proc. 2003 Particle Accelerator Conference,* Portland, OR, May 2003.

16. CST Microwave Studio, Computer Simulation Technology (http://www.cst.de/)
17. Kenneth W. Shepard, "The RIA Driver Linac", *Proc. 2002 Linear Accelerator Conference,* Gyeongju, South Korea, August 2002.
18. I. E. Campisi, et al., "Results Cryogenic Testing SNS Prototype Cryomodule", *Proc. 2002 Linear Accelerator Conference,* Gyeongju, South Korea, August 2002.
19. T. Tajima, et al., "Test Results LANL Beta=0.175 Two-gap Spoke Resonator", *Proc. 2002 Linear Accelerator Conference,* Gyeongju, South Korea, August 2002.
20. W. Hartung, et al., "Status Report on Multi-Cell Superconducting Cavity Development for Medium-Velocity Beams", *Proc. 2003 Part. Acc. Conf.*, Portland, OR, May 2003.
21. R. A. Byrns and M. A. Green, *Adv. Cryo. Eng.* **43**, p1661 (1998).
22. V. Ganni, private communication.
23. E.P. Knapp, in *Proc. 1971 Particle Accelerator Conference,* IEEE Trans, Nucl. Sci. NS-18, no.3, p.508. 1971.
24. S.K. Esin, L.V. Kravchuk, V.A. Matveev, P.N. Ostroumov and V.L. Serov, *Proc. 1994 Linear Accelerator Conference*, edited by K. Takata et al, August 21-28, Tsukuba, Japan, pp. 31-35.
25. R.J. Noble, *Proc. 1992 Linear Accelerator Conference*, edited by C.R. Hoffmann, August 24-28, Ottawa, Ontario, Canada, AECL-10728, p. 565.
26. Y. Yamazaki, et al. *Proc. 1999 Particle Accelerator Conference, edited by A. Luccio and W. MacKay,* NY, 1999, p. 513.
27. P. N. Ostroumov and K. W. Shepard, Phys. Rev. ST Accel. Beams **3**, 030101 (2000).
28. P. Ostroumov, et al., "Design of 57.5 MHz CW RFQ for Medium Energy Heavy Ion Superconducting Linac"; Phys. Rev. ST Accel. Beams **5**, 060101 (2002)
29. P.N. Ostroumov, "Sources of Beam Halo Formation in Heavy-Ion Superconducting Linac", in *Proc. ICFA Advanced Beam Dynamics Workshop "Halo'03",* May 19 - 23, 2003, Montauk, N.Y.
30. D. Berkovits and A. Facco, "Stripping effects in a heavy ion linacs". LNL-INFN (REP) 191/2002.
31. J.F. Ziegler, J.P Biersack, U. Littmark, "The Stopping and Range of Ions in Solids", Pergamon Press, New York (1985); Program SRIM, J.F. Ziegler, IBM-Research